AC motor impedance predictive modeling methodology taking into account windings variability

Arthur Piat, Pierre-Etienne Lévy, Sami Hlioui, François Costa, Sébastien Serpaud

Submitted to **Journal Title**
Template provided by EDP Sciences

RESEARCH ARTICLE

AC motor impedance predictive modeling methodology taking into account windings variability

A. Piat[1,2*], P.-E Lévy[1], S. Hlioui[3**], F. Costa[4], and S. Serpaud[2]

[1] SATIE, CNRS, Paris Saclay University, ENS Paris Saclay, 91190 Gif-sur-Yvette, France
[2] Institut de Recherche Technologique Saint Exupéry, 31400 Toulouse, France
[3] SATIE, CNRS, CY Cergy Paris University, Paris Saclay University, 95000, Cergy, France
[4] SATIE, CNRS, Paris Est Créteil University, Paris Saclay university, Créteil, France

Abstract – This paper presents a unified predictive modeling for common-mode (CM) and differential-mode (DM) impedance estimation of a Permanent Magnet Synchronous Motor (PMSM). This methodology combines 2D Finite Element modeling and generated lumped parameter circuit in Spice environment. It is then used to determine the consequences of design choices and evaluate the importance of controlling the winding process in the PMSM manufacturing. By doing so and by changing parts of the PMSM design, the overall high frequency response of the system with regards to input parameters can help in satisfying EMC high frequency constraints (between 1 kHz and 10 MHz).This paper presents evidences demonstrating the importance of design parameter such as the number of wire in parallel used by turns and the overall placement of conductor not only with regards to the slot, but to other wires within the slot

Keywords. Electromagnetic Compatibility (EMC), common-mode (CM), differential-mode (DM), electrical machine, HF modeling, finite element method

1. Introduction

In recent years, the trend in embedding electric systems in aircraft has allowed performance gains by reducing both the weight and the size of hydraulic or pneumatic systems [1]. Increasing electrical systems power density is a key challenge to replace high-power functions, therefore Wide-band gap semiconductor such as SiC and GaN became a key factor to reach higher thresholds of power transmission and reduce losses by working at higher switching frequency [2]. However, increasing switching frequency and switching times enhance the spectrum of Electromagnetic Interferences (EMI) generated [3]. These disruptions can spread everywhere the system and even to neighboring devices. The propagation paths and dangers of such currents are well known and have been the subject of numerous experimental and measurement-based articles [4–8].

As these currents can generate disturbances for neighboring systems [9], they are to be limited following various regulations [10], generally using filtering devices. Behavioral models can be created using series of measurements [11–14] to size passive filtering systems on existing systems, requiring a working prototype. Predictive modeling using Finite Element Methods (FEM) allowed predicting cable behavior [3] and this method was naturally used to evaluate electrical machine behavior at a broad spectrum of frequencies (few kHz up to 10 MHz) both in CM and DM [14–16] as well as estimating overvoltage within stator windings [17–19]. CM capacitance estimation of a motor using probability density function showed variations in capacitance with various filling patterns [20]. However, the association of wire in parallel as well as the wire turns's relative position to each other are not covered.

In this paper, a methodology, combining FEM and Spice circuit modeling, to predict both CM and DM impedances on a frequency spectrum between 1 kHz up to 10 MHz is described. Using this methodology with various windings, a better understanding of the variables to be adjusted to adapt both CM and DM impedance frequency spectrum of a PMSM is proposed. Firstly, design variables will be presented and the motivation toward such parameters. The global simulation process allowing impedance prediction will be highlighted. Parametric studies are then presented with regards to the number of wire used in parallel and winding placement withing the slot. Finally, a preliminary experimental validation is shown, proving the need to address such parameters both in modeling and manufacturing processes.

* Corresponding author: arthur.piat@irt-saintexupery.com
** Corresponding author: sami.hlioui@ens-paris-saclay.fr

2. Modeling and hypotheses

To study the impact of PMSM design variables, a model needs to be parametrized and computed in various configurations. A use case of a PMSM with a fixed slot form is selected. Only the winding is changed with regard to four parameters.

2.1. Number of wires in parallel

For a given power, a similar electrical machine can be created using different wires. Using wires in parallel, manufacturers can both wind stators more easily than with a large single and therefore more rigid wire, as well as reducing losses due to skin and proximity effects. It is often assumed that thermal constraints will remain similar if the same equivalent copper surface is kept. A hypothesis is that parallel wires are considered at the same impedance at any frequency.

2.2. Dispersion between groups of wires

During the manufacturing process, wires wounded in parallel may not stay in a perfectly stacked group, some wires may be mixed with other groups and will not form a perfect packing pattern. This difference induces a different level of interaction between each group (magnetic and capacitive) that needs to be evaluated. The importance of such interactions in HF CM and DM modeling is yet to be quantified.

2.3. Order and position of wire groups in slots

In a stator slot or winded rotor, the position of wire groups in a slot is heavily dependent on the manufacturing process, and this order can have significant consequences on partial discharge and voltage levels between turns [18]. Their consequences on CM and DM are yet to be quantified.

2.3.1. Packing of wires within slots

Wires, when placed in a slot, do not fill the form in perfect hexagonal or square patterns that can significantly change low frequency and high frequency behavior of the system [20]. This aspect will be partially addressed here.

A general workflow, presented in Figure 1., allows considering all those parameters. The first step consists in defining a simplified geometry for the slot, only composed of lines (Illustrated by step 1 Figure 1). This allows dividing the overall space and defining potential places for conductors. A mesh (different from FEM mesh) is refined until all conductors fit within a slot (Illustrated by step 2 Figure 1). This allows changing between wire configurations (diameter and number). If a mesh allows for more than the needed number of wires, extra positions are randomly selected and removed (Illustrated by step 3 Figure 1). This algorithm will fill any slot volume with an hexagonal pattern.

Afterwards, groups need to be defined, as wires in the same group are representing wires winded in parallel in the real motor. The variables $N_{\text{var group}}$ modify the way wires are grouped based on their relative distance: if $N_{\text{var group}}$ is equal to zero, only the closest wires are selected to be part of a group, if $N_{\text{var group}}$ is equal to the number of conductors, every conductor can be in any groups. For instance, in step 4 Figure 1, $N_{\text{var group}}$ is equal to zero and groups of two wires are created, starting from the bottom center of the slot, the closest wire is grouped with its closest neighbor until all wires have a group. Finally, N_{added} will randomly switch groups order depending on the given value. This allows for variability in association and organization but do not change conductors' position. As shown in step 5 Figure 1, if N_{added} is equal to one, an inversion of group order can be observed randomly. This process was designed to maximize the repartition within slot, by creating such mesh, we are forcing all conductors to be separated in average by the maximal distance possible. Such filling strategy is not entirely representative to the configuration found in real motors as the manufacturing process can spatially move any wire and is not the same throughout the motor length [20] but allow for variation studies in winding. Once this workflow has modified the overall winding, a following workflow will allow extracting HF impedance similar to [14–16].

3. FE simulations for impedance extraction

The geometry defined by the algorithm will be used to generate three FE models: two magnetic analyses and an electrostatic one using FEMM [21]. As the 2D nature of these tools cannot replicate the complexity of real electrical machines, hypotheses were taken. Indeed, contrary to [16], the studied motor end-windings lengths are not negligible, inducing a significant number of turn-to-turn capacitance and inductances in the overall motor winding.

3.1. Magnetic model for slot resistance and inductance

A section of the motor is drawn with a pole. As this PMSM only have one phase by slot, only two windings are represented to form the global induction loop Figure 2. All groups are excited one by one with a 1A current to extract self and mutual impedances. For a given configuration of winding, all conductors in the same group are considered in parallel therefore the current is applied to all conductors leading to an overall impedance. By dividing the voltage drop, noted ΔV, by the total current I_i flowing thought conductors in group i, resistance R and mutual- as well as self-inductance L matrices are computed using equations 1 and 2.

$$L_{ij} = imag(\Delta V_j / I_i)/\omega \tag{1}$$

$$R_{ij} = real(\Delta V_j / I_i) \tag{2}$$

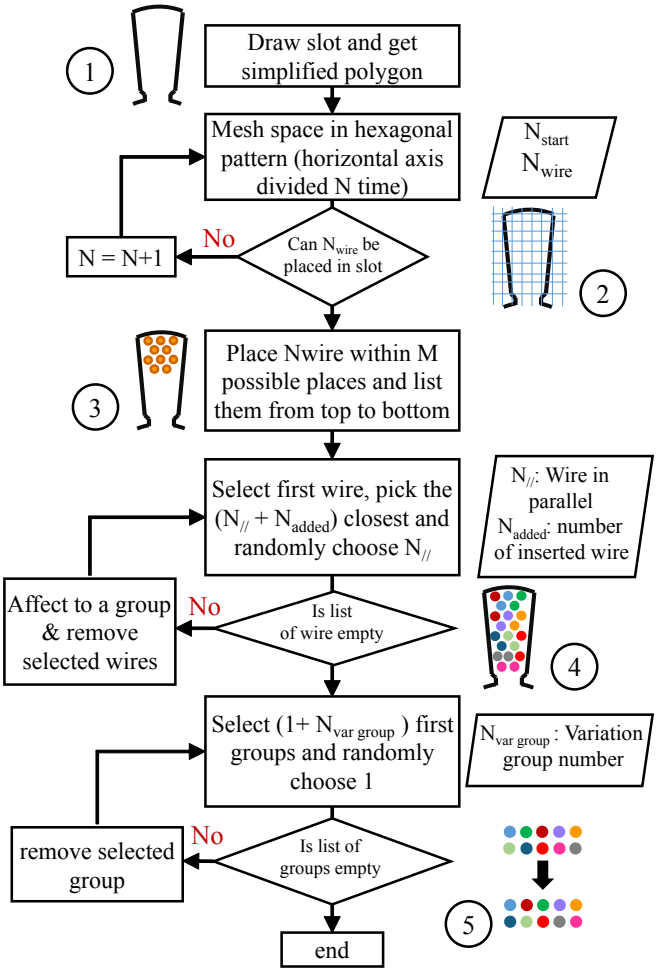

Figure 1. General workflow for winding randomization

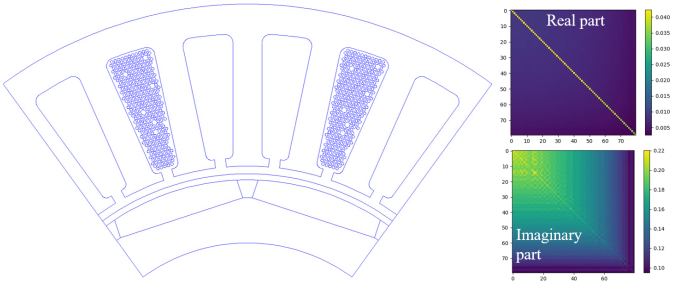

Figure 2. Slot impedance characterization with FEMM

i: Group with 1A imposed current, $\omega = 2\pi f$

For this simulation, insulation on the wire and in the slot is not represented as they behave very similarly to the air. Meshing is adapted with regard to skin depth to extract coherent values. Magnetic simulations are performed up to 10 MHz, resulting in more computationally intensive simulations at high frequency and in some cases instability in FEMM software as the mesh on wire circumferences is refined. Consequently, simulations do not exceed 10 MHz. Finally, to consider the machine magnetization stack created by magnets, a simulation is performed beforehand without any current. The magnetic circuit characteristics are imported afterwards using the frozen permeability feature of FEMM software.

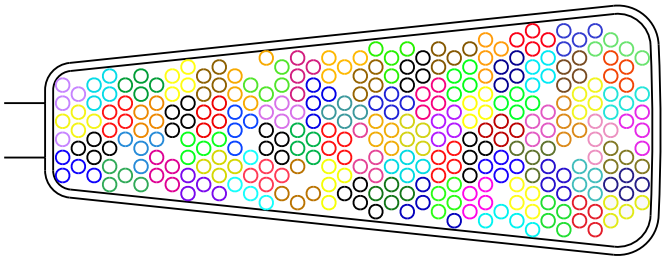

Figure 3. Illustration of capacitive model with no enamel, featuring wire groups

3.2. Capacitive model for turn-to-turn and turn-to-ground

Regarding capacitive computation, the process is similar to inductance and resistance estimation. All conductors in one group (shown by colors, Figure 3) have their surfaces excited at 1 V, noted V_i , in an electrostatic simulation while all others, as well as the slot border, are fixed at 0 V. Capacitance's matrices C are therefore computed dividing surface charges q_j on conductor j by V_i as shown on equation 3. It is to be noted that in case of i=j, the capacitance is in fact $C_{i\text{-ground}}$ meaning the capacitance between the group i and the slot surface.

$$C_{ij} = q_j / V_i \tag{3}$$

i: Group with 1V imposed excitation

3.3. Magnetic and electrostatic models for end-windings

The total length of the studied motor is composed of one third of end-winding. Consequently an end-winding model was developed. However, using 2D FEM models, hypotheses need to be taken. The chosen approach uses an axisymmetric model, all conductors are kept in the same position as within the slot featured Figure 3 and the distance to the revolution axis is half the distance between the two slots used by one coil, creating half a circle to create a circularly ideal end-winding. Coupling inductances between different phases are likewise considered negligible. Finally, inductances and resistances as well as capacitances are computed, similarly to their slot counterpart using 1, 2 and 3 equations.

For the following results, the values chosen are: copper electrical conductivity, 58 MS/m and relative permittivity equal to 1. M-36 Steel FEMM default material with a relative permittivity of 2.164. Wire insulation and slot insulation layer have both an electrical conductivity of 0 MS/m (like air) but a relative permittivity of 5.

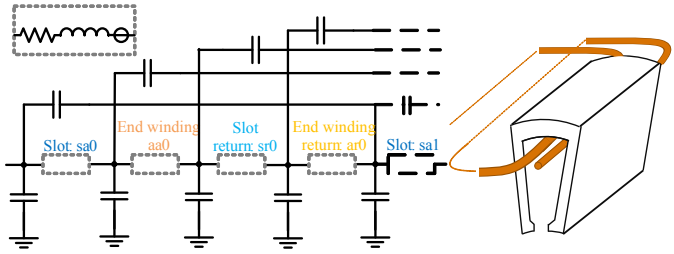

Figure 4. Schematic spice used for circuit construction with matching 3D slot representation

4. Spice circuit generation

All FEM simulations need to be integrated in an overall circuit to allow CM and DM impedance characterization. The electric model corresponding to one slot of Figure 4 with associated nomenclature of Table 1. are presented for a motor with a single phase by slot. Two main repeating units compose this circuit:

Table 1. Nomenclature used for lumped parameters

Type	Element: L, R, k, C, V for inductances, resistance, coupling coefficient, capacitances and real impedance coupled generators
Position	Position indices in loop: s for slot, a for air
Direction	Direction: a for first half of loop, r for return
Number	Number of completed loops (starting at 0) If only a number is given: self-property If two numbers are given: coupled property
Examples Csa0_5: Capacitance between wires 0 and 5 in first slot Lar8: Self-inductance of wire 8 in return end-winding Vaa6: Real impedance of group 6 in first end-winding	

4.1. Slot model with capacitive and inductive coupling

Ls and Rs components are respectively filled using R_{ii} and L_{ii} from equations 1 and 2; similarly C_s is derived from equation 3. As one coil will go through two slots, this part needs to be repeated twice to get the desired behavior (Lsa - Lsr, Rsa-Rsr and Csa-Csr). Finally, as this repeating unit is used for each turn in the electrical motor slot, mutual inductances between each group are implemented using equation 4 as Spice solver uses coupling factors and not mutual impedances. These coupling coefficients are named Ksa, Ksr, Kaa and Kar matching the previous notation.

$$k_{ij} = L_{ij}/\sqrt{L_{jj}.L_{ii}} \tag{4}$$

4.2. Coupled real impedance generators

To add the real part of the coupled impedance, no passive components exist apart from coupling factor in inductances. The real part of coupled impedances can be represented using behavioral voltage sources in the Spice simulator. The schematic described in [16] is not easily implementable in previous developed workflow therefore the equation 5 was used:

$$V_j = \sum I_j.R_{ij}, \forall i \neq j \tag{5}$$

One behavioral voltage source is used for each wire but the expression depends on the current within other groups. This source acts very similarly to coupling coefficient for inductances and will "transfer" energy from one wire group to other groups. Similarly, coupling coefficient between inductances are placed for each conductor at every turn of the winding. The nomenclature adopted is Vsa, Vsr, Vaa and Var.

4.3. End winding model

Similarly to their slot counterpart, resistor, inductance, coupling coefficient and capacitances are used for both sides of the electrical machine (respectively Raa, Rar and Laa, Lar, Kaa, Kar and Caa, Car).

A resulting circuit is generated for each frequency point simulated and solved by LTSpice, capacitive couplings are considered constant at each frequency while resistance and inductance are highly impacted by skin and proximity effect. FEMM magnetic models are simulated at various frequencies and matrices are linearly interpolated to obtain in between values. Laplace voltage-controlled generators were investigated similarly to [16] but due to the extensive number of expressions needed for an eighty-turn electrical machine, the previous approach was preferred. Within these netlist, a voltage generator is placed either between ground and sa0 (node at the beginning of the coil) or between sa0 and arN (N being the number of turns) for respectively Common-mode and Differential-mode impedance characterization. Combining these values and matching measurement on existing motor will allow validating the overall approach, similarly to [14–16].

5. Studied configurations and HF trade-off

Three configurations are studied, depicted in Table 2. The aim is to compare three electrical machines considered equivalent from a mechanical standpoint but with different types of winding. The chosen enamel thickness matches the average IEC 06317 Grade 2, apart from S3 which is an estimated value to keep the same copper surface for all tested values. All these configurations are simulated with tools described before, allowing plotting both CM and DM impedances. The following comparisons are based on a single coil and not on a full motor. On Figure 5, Table 2 configurations are simulated, configuration S1 is plotted in blue, S2 in orange and S3 in red. Configurations S1-w/V to S3-w/V feature impedances computed without voltage controlled sources representing proximity effects, differences with S1 to S3 are discussed Section 5.4. Finally, lumped parameters are computed in Table 3 for comparison.

Table 2. Studied PMSM winding configurations

Reference	Design variables		
	Winding copper diameter	Enamel thickness	Wire in parallel
S1	1.0 mm	0.08 mm	1
S2	0.5 mm	0.055 mm	4
S3	0.25 mm	0.041 mm	16

Table 3. Nomenclature used for lumped parameters

Reference	Estimated lumped parameters		
	CM capacitance	DM inductance	AC resistance[1] (1 MHz)
S1	82.8 pF	3.11 mH	44.8 Ω
S2	137 pF	3.09 mH	39.3 Ω
S3	216 pF	3.07 mH	38.7 Ω

[1] defined in subsection 5.3

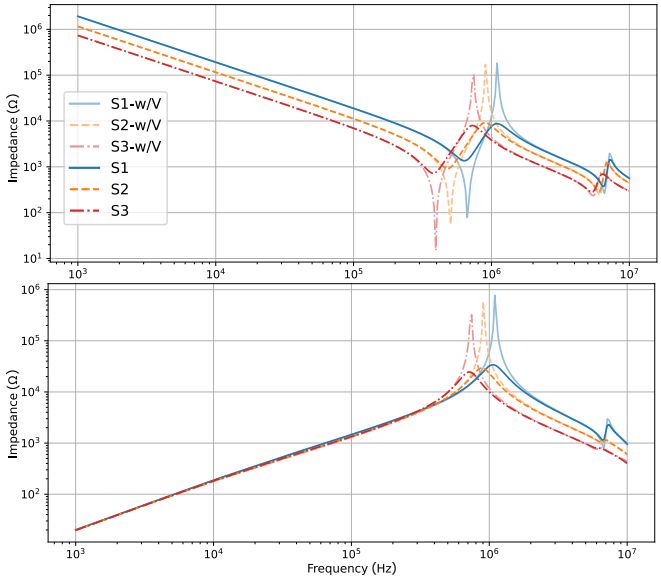

Figure 5. CM and DM impedance of a simulated 80 turn coil within a stator using different winding

5.1. Common mode impedance

The common mode capacitance is the low frequency capacitance that can be seen on the upper graph Figure 5. It is computed with either Spice simulation or using capacitance matrix trace. As more parallel conductors are used, more energy is stored between wires and the slot. This can be explained as the small wire tend to fill more the space around the slot edge, resulting in an increase of the capacitance between groups and the slot surface. Moreover, the enamel thickness does not decrease proportionally to the copper diameter, resulting in a bigger proportion of material with a high relative permittivity.

5.2. Differential mode inductance

Similarly to CM capacitance, DM inductances are estimated using the first part of curves on the lower graph Figure 5. However, computing it from matrices can be difficult as coupled inductances impact the slope at the first order. This value does not vary significantly from configuration S1 to S3.

5.3. AC resistance of coil

AC resistance is estimated as the sum of all resistances in series in the circuit Figure 5, or more simply the trace of matrix R, equation 2 at a given frequency. At this value is highly frequency dependents, a comparison between configurations is performed at 1 MHz. As this frequency, both skin and proximity effect highly impact the overall value. By computing the trace of the matrix resistance, it appears as if loss remains similar for every configuration. This result may appear counterintuitive to the fact that reducing wire diameter (such as using Litz wires) reduces losses [22], but these observations are made at the motor working frequency and not at high frequencies studied in this paper.

5.4. Real impedance coupled voltage generators

In preliminary result, the real part of coupled impedances was neglected similarly to [14] as no behavioral voltage sources were used. As seen on Figure 5, such circuit presented resonances with no damping (see S3-w/V compared to S3). In [14, 15], the damping was not present in the curves obtained as no dielectric and iron losses were modeled. However, results presented in [16] have significant damping due to coupled real impedances but do not use any dielectric losses. Both authors in [14] and [23] noted a significant difference between their models and impedance measurements in particular on damping. No conclusion can be drawn to this question in the current study and further work is needed to conclude on the need to combine those aspects as no dielectric losses were taken into account in this paper. By comparing the curve from S1 to S3, not a significant difference in damping can be observed between each configuration. The origin of such losses can be linked to induced current within other wires, coupled with proximity and skin effect. However as the frequency increases, the damping on resonances returns to the level of simulations without voltage source, reducing the need to include the real part of coupled impedances in spice netlist.

5.5. General remarks on impedance curves and resonances

Regarding common mode, the low frequency capacitance seen on the various curves is driven by the capacitances of wires to slots, the first resonance is linked to both the line inductance (DM inductance in Table 3) and turn-to-turn capacitances [22]. As this inductance remains the same for all configurations and turn-to-turn capacitance is minimized due to the topology simulated, the first resonance is moved to lower frequencies whenever the CM capacitance is increased. The second resonance on CM impedance is more complex: as a difference

in potential appears between each turn, a new association of capacitance is excited combining turn-to turn and turn-to-slot capacitances. Following resonances are higher modes of the transmission line behavior of the system between the non-linear inductances of wires due to skin and proximity effect and all capacitances. The DM inductance computed Table 3 drives DM impedances for the most part, skin and proximity effect change the value of self and mutual inductances, this results in a slight decline from the expected 20dB/decade slope, up until the first resonance with turn-to-turn capacitances change the behavior of the curve. Resonance frequencies match the CM impedance curve, resulting in similar behavior in both curves after the second and first resonance from CM and DM impedances respectively, implying that turn-to-turn capacitance is the main factor determining the first DM impedance resonance frequency in this winding configuration. A sensibility analysis was performed to validate the impact of such capacitance on impedance value Section 6.

6. Sensibility analysis to turns dispersion

The studied PMSM studied in this paper uses random wound : coils placed within the stator are mechanically formed by hand or by an automated production line and placed in the stator. The exact place at which each conductor is moved is undetermined. General guidelines may be given to minimize overvoltage and differential tension between turns such as in [18, 19] but the exact whereabouts of each conductor is not known. To tackle this issue and understand the impact of such dispersion, a sensibility analysis was performed using only configuration S2 from Table 2. The studied configurations are regrouped in Table 4 and shown on Figure 6. The color of each wire on Figure 6 represents groups of wires in parallel. Configuration B1 is equivalent to Figure 3 S2 and features an ideal configuration where all wires are not mixed and turns with similar order remains adjacent to each others (the first turn is close to the second and third turn for instance) meanwhile configuration B2 and B3 degrade those factors, leading to B4 exhibiting the worst-case scenario. Impedance curves displayed Figure 7 were obtained using the identical process as outlined before for configurations S1 to S3.

Table 4. Winding configurations for random wound

Reference	Design variables		
	Windings	N_{added}	$N_{var\ group}$
B1 (S2)	4 wires, 0.5mm	0	0
B2	4 wires, 0.5 mm	2	4
B3	4 wires, 0.5 mm	3	6
B4	4 wires, 0.5 mm	max	max

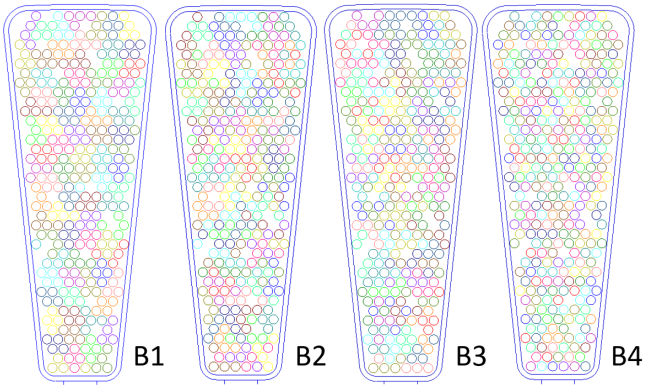

Figure 6. B1 to B4 coil illustration with wire groups, without enamel

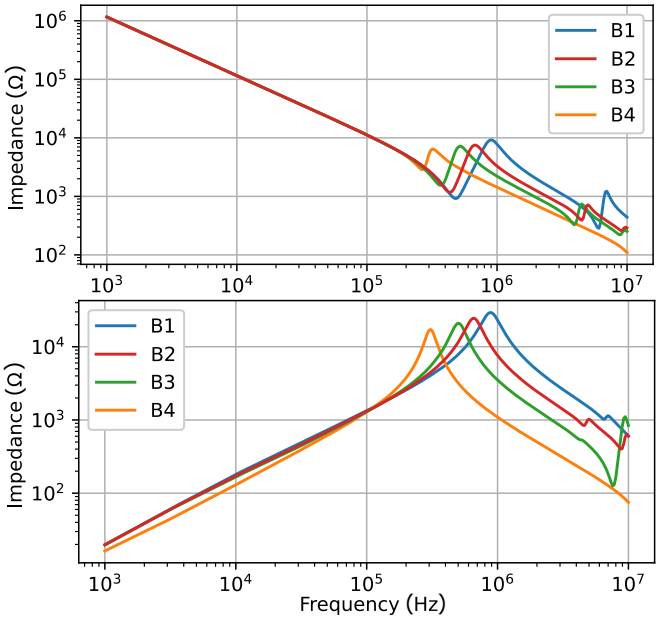

Figure 7. CM and DM impedances with different winding configurations

6.1. Impedance modification due to variation in windings

Figure 7 displays both DM and CM impedance norms. B1 curves are equivalent to Figure 5 S2 simulations. With each configuration, as wires become increasingly shuffled within the slot, the first resonances are displaced at lower frequency. This phenomenon arises from the alteration of turn-to-turn capacitance between each configuration meanwhile the overall turn-to-slot capacitance are kept the same resulting in low frequency CM impedance value equal across all configurations. These observations provide further support for those made in [24]. Moreover, proximity effects can have a non-negligible impact on lower frequency inductances as shown by configuration B4 on DM impedance. Yet, for more realistic configurations (B1, B2 and B3), this disparity seems negligible on

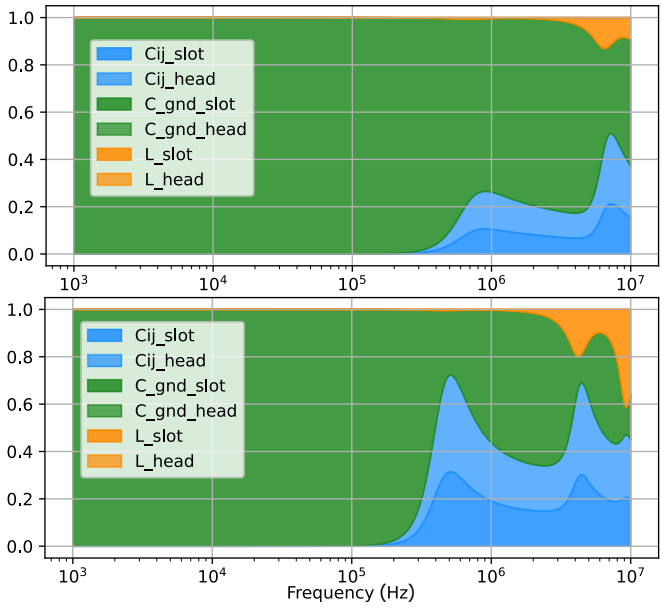

Figure 8. Energy ratio for CM impedance, configuration B1 and B3

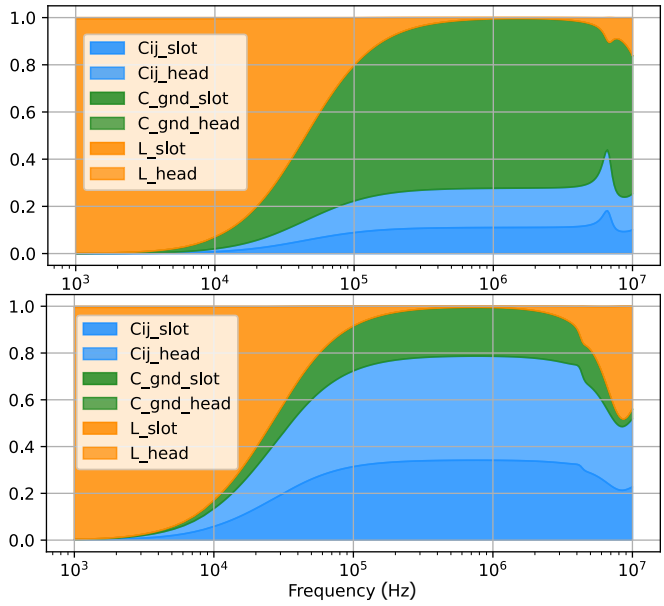

Figure 9. Energy ratio for DM impedance, configuration B1 and B3

impedance value. Controlling the displacement of windings within the overall manufacturing process is therefore important to reduce insulation stress caused by dV/dt [18, 19] but also for reducing CM filtering devices.

6.2. Energetic contribution to impedance value

To visualize in more depth the contribution of each element (capacitances, inductances) to the overall impedance, the energy stored in the overall spice schematic is computed and classed in three categories (inductance, capacitance wires to ground, capacitance turn-to-turn) separated between slot and end-winding, resulting in a total of six categories. The accumulated stored energy is summed and shown at each frequency and normalized to compare every winding configuration. Figure 8 and Figure 9 features winding B1 and B3 in CM and DM. Energy diagrams confirm that low frequency CM impedance is driven by turn-to-slot capacitance, until the first resonance which features a different contribution depending on turn-to-turn capacitances, B1 impedance being driven by turn-to-slot capacitance meanwhile turn-to-turn capacitance makes the major contribution to B3 impedance after the first resonance. Similarities can be found on the DM impedance: low frequency behavior is dictated by the inductance within the iron stack, as frequency increases, the contribution of turn-to-slot and turn-to-turn capacitance becomes more preponderant.

7. Experimental validation

To validate these findings, prototypes were developed to assess the influence of design decisions. A non-functional stator was assembled with nine coils. Three of each winding configuration (S1 to S3) and mechanically

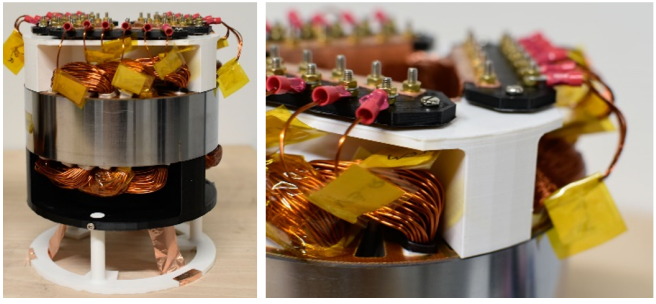

Figure 10. S1 to S3 windings assembled on a stator for validation

assembled to facilitate consistent measurements as featured on Figure 10. These windings were measured using and impedance analyzer, between coils input and output and between coils input and stator iron stack to replicated DM and CM simulations respectively. The ground reference is the iron stack as the copper plate connected on each terminal block is electrically connected to iron sheets using copper tape. Experimental results are displayed Figure 11 alongside simulations.

As featured on Figure 11, the winding featuring the highest resonance frequencies was correctly identified and the evolution associated with the number of wires in parallel was accurately predicted, allowing designers to take into consideration EMC constraints at preliminary design stages. There is a distinct disparity between simulation and hand-on experiments, factors responsible for such differences are the placement of conductors: wire-to-slot capacitances is not fully represented as the filling algorithm tries to fill the slot uniformly but a denser pattern can appear toward some parts the slot [20]. Furthermore, turn-to-turn capacitances in these simulations are minimized due to a wire groupings analogous to B1 Figure 6,

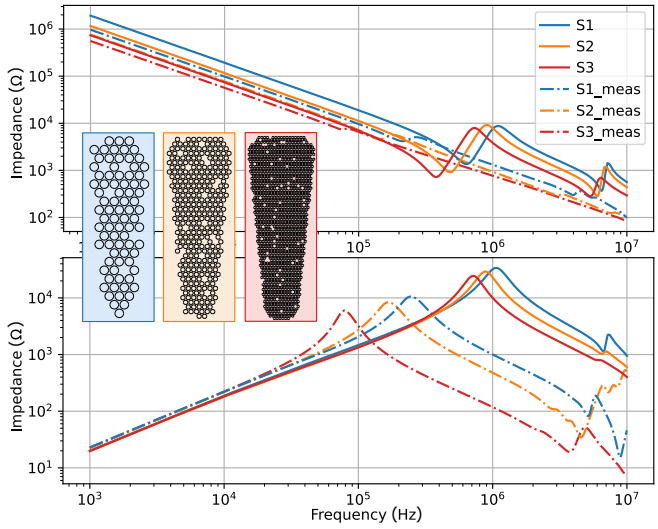

Figure 11. Simulation and measurements for CM and DM impedance for S1 to S3 windings

it can indeed significantly reduce the frequency at which the first resonance can be seen as shown in Section 6 and [26].

8. Conclusion

In this paper, HF identification and simulation methodologies for various PMSM winding types were developed and tested. A geometry is generated with an associated winding, simulated using FEM and equivalent impedance measurements are performed. This process is then used to evaluate the impact of wire in parallel and dispersion within slots. Finally, predictions are compared to measurements done on validation stators. Results shows that increasing the number of wires in parallel for a given configuration of slots and turns number carry a substantial risk to reduce the resonances frequency mainly driven by wire to slot capacitance. These phenomena will directly influence the system response to various regulations [10]. Further work is needed: dielectric losses need to be integrated to represent more accurately the resonance amplitudes and a physical model for wire placement and association would increase the accuracy of impedance values computed. Meanwhile, assessing the consequences of this behavior on the entire power drive and filtering devices will enlighten which trade-off needs to be made to improve global performances, with regard to regulation and system constraints. The robustness of such trade-off needs to be tested by introducing uncertainties in the winding that will represent the variations induced by fabrication processes. Finally, measurements and experiments allowed to validate the evolution of impedances with regard to wires in parallel, despite differences manly linked to random placement and displacement of wire within the slot.

Acknowledgements

This paper is part of the OCEANE Project led by IRT Saint Exupéry, Toulouse (France), which is sponsored by AIRBUS, LIEBHERR, SAFRAN and the French National Research Agency (ANR) in collaboration with SATIE, TUD, DEEP, ICAM and LAPLACE.

References

1. Berger R., Nazukin M., Sachdeva N. and Martinez N. (2017) Think: Act Aircraft Electrical Propulsion - The Next Chapter of Aviation ?, Roland Berger LTD
2. Sathler H. H. (2021) Optimization of GaN-based Series-Parallel Multilevel Three-Phase Inverter for Aircraft applications, PhD Thesis. Université Paris-Saclay, Gif-sur-Yvette, 284p
3. Dos Santos V. (2019) Conducted electromagnetic emissions modeling in adjustable speed motor drive systems. Parametric studies and optimization of an inverter and filters under EMC constraints, PhD Thesis. INPT, Toulouse, 298p
4. Hadden T. et al. (2016) A Review of Shaft Voltages and Bearing Currents in EV and HEV Motors, in: IECON 2016 - 42nd Annual Conference of the IEEE Industrial Electronics Society, pp. 1578–1583. https://doi.org/10.1109/IECON.2016.7793357
5. Costello M. J. (1993) Shaft voltages and rotating machinery, in: IEEE Trans. Ind. Appl., vol. 29, no. 2, pp. 419–426, https://doi.org/10.1109/28.216553
6. Plazenet T., Boileau T., Caironi C., and Nahid-Mobarakeh B. (2018) A Comprehensive Study on Shaft Voltages and Bearing Currents in Rotating Machines, in: IEEE Trans. Ind. Appl., vol. 54, no. 4, pp. 3749–3759, https://doi.org/10.1109/TIA.2018.2818663
7. Asefi M. and Nazarzadeh J., (2017) Survey on high-frequency models of PWM electric drives for shaft voltage and bearing current analysis in: IET Electr. Syst. Transp., vol. 7, no. 3, pp. 179–189, https://doi.org/10.1049/iet-est.2016.0051
8. Shami U. T. and Akagi H. (2010) Identification and Discussion of the Origin of a Shaft End-to-End Voltage in an Inverter-Driven Motor, in : IEEE Trans. Power Electron., vol. 25, no. 6, pp. 1615–1625, https://doi.org/10.1109/TPEL.2009.2039582
9. Morgan, D., and Mulhall B. (1995) A Handbook for EMC Testing and Measurement. IOP Publishing, Bristol, Measurement Science and Technology 6.5: 600.
10. Mariscotti A., and Leonardo S. (2021) Review of models and measurement methods for compliance of electromagnetic emissions of electric machines and drives, ACTA IMEKO, **10**, 2, 162-173
11. Zhao D., Shen K., Liu W., Lang L. and Liang P. (2019) A Measurement-Based Wide-Frequency Model for Aircraft Wound-Rotor Synchronous Machine, in: IEEE Transactions on Magnetics, vol. 55, no. 7, pp. 1-8, Art no. 8105408, https://doi.org/10.1109/TMAG.2019.2900616
12. Maki K., Funato H. and Shao L. (2009) Motor modeling for EMC simulation by 3-D electromagnetic field analysis, in: IEEE International Electric Machines and Drives Conference, pp. 103-108, https://doi.org/10.1109/IEMDC.2009.5075190
13. Gries M. A. and Mirafzal B., (2008) Permanent Magnet Motor-Drive Frequency Response Characterization for

Transient Phenomena and Conducted EMI Analysis, in: IEEE APEC 2008, pp.1767-1775.
14. Boucenna N. (2014) HF common mode EMC modeling of AC three-phase motors, PhD Thesis. École normale supérieure de Cachan-ENS Cachan, Cachan, 166p
15. Boucenna N., Costa F., Hlioui S. and Revol B. (2016) Strategy for Predictive Modeling of the Common-Mode Impedance of the Stator Coils in AC Machines, in: IEEE Transactions on Industrial Electronics, vol. 63, no. 12, pp. 7360-7371, https://doi.org/10.1109/TIE.2016.2594052
16. Ruiz-Sarrió J. E., Chauvicourt F., Gyselinck J. and Martis C. (2021) High-Frequency Modelling of Electrical Machine Windings Using Numerical Methods, in: IEEE International Electric Machines & Drives Conference (IEMDC), pp. 1-7, https://doi.org/10.1109/IEMDC47953.2021.9449561
17. Pastura M. et al. (2021) Partial Discharges in Electrical Machines for the More Electric Aircraft—Part I: A Comprehensive Modeling Tool for the Characterization of Electric Drives Based on Fast Switching Semiconductors, in: IEEE Access, vol. 9, pp. 27109-27121, https://doi.org/10.1109/ACCESS.2021.3058083
18. Mihaila V. (2011) New conception for AC machine's stator winding minimizing dV/Dt, PhD Thesis. Université d'Artois, Artois, 148p
19. Mihaila V., Duchesne S. and Roger D. (2011) A simulation method to predict the turn-to-turn voltage spikes in a PWM fed motor winding, in: IEEE Transactions on Dielectrics and Electrical Insulation, vol. 18, no. 5, pp. 1609-1615,https://doi.org/10.1109/TDEI.2011.6032831
20. Hoffmann A., Knebusch B., Stockbrügger J. O., Dittmann J. and Ponick B. (2021) High-Frequency Analysis of Electrical Machines Using Probability Density Functions for an Automated Conductor Placement of Random-Wound Windings, in: IEEE International Electric Machines & Drives Conference (IEMDC) pp. 1-7, https://doi.org/10.1109/IEMDC47953.2021.9449557
21. Meeker D. (2020) "Finite element method magnetics," FEMM, vol. 4, p. 161
22. Pechlivanidou M. S. C. and Kladas A. G. (2021) Litz Wire Strand Shape Impact Analysis on AC Losses of High-Speed Permanent Magnet Synchronous Motors, in: 2021 IEEE Workshop on Electrical Machines Design, Control and Diagnosis (WEMDCD), pp. 95-100, https://doi.org/10.1109/WEMDCD51469.2021.9425656
23. Ruiz-Sarrió J. E., et al (2023) Impedance Modelling Oriented Towards the Early Prediction of High-Frequency Response for Permanent Magnet Synchronous Machines, in: IEEE Transactions on Industrial Electronics. vol. 70, no. 5, pp. 4548-4557, https://doi.org/10.1109/TIE.2022.3189075
24. Vostrov K., Pyrhönen J. and Ahola J. (2019) The Role of End-Winding in Building Up Parasitic Capacitances in Induction Motors, in: 2019 IEEE International Electric Machines & Drives Conference (IEMDC), San Diego, CA, USA, pp. 154-159, https://doi.org/10.1109/IEMDC.2019.8785238
25. Li J., Liu R., Zheng B. and Zhang Y. (2012) The effects of end part of winding on parasitic capacitances of induction motor fed by PWM inverter, in: 2012 15th International Conference on Electrical Machines and Systems (ICEMS), Sapporo, Japan, 2012, pp. 1-5.
26. Ruiz-Sarrió J. E., Chauvicourt F. and Martis C. (2022) Sensitivity Analysis of a Numerical High-Frequency Impedance Model for Rotating Electrical Machines, in: 2022 International Conference on Electrical Machines (ICEM), Valencia, Spain, 2022, pp. 1260-1266, https://doi.org/10.1109/ICEM51905.2022.9910666